

# Hidden Thresholds: A Technique for Reconstructing New Physics Masses at Hadron Colliders

P. Huang, N. Kersting<sup>1</sup>, H.H. Yang

*Physics Department, Sichuan University, P.R. China 610065*

## Abstract

We present a completely general method of reconstructing all New Physics (NP) masses in semi-inclusive processes of the form *anything*  $\rightarrow$  NP  $\rightarrow$  jets + leptons. For calculational purposes, "anything" consists of a set of auxiliary particles  $X_i$  whose masses sum to threshold production of NP. There are then three steps to find NP masses: [1] DEFINE the specific decay chain leading from NP to the hard jets and isolated leptons; [2] DERIVE analytic expressions for all jet and lepton invariant mass endpoints as functions of NP masses, and find kinematic configurations for which two or more of these are co-extremal; [3] DISPLAY correlations of the above invariants in a plot which makes their extremal values visually obvious and easily computable. This technique works because geometric features marking extremal values are fortified when superimposed with decays where the  $X_i$  are away from threshold, which is precisely the situation at a hadron collider such as the Tevatron or the LHC. Background effects (mostly from competing NP decay chains) are minimal since these will not have the correct correlations among invariants. We illustrate this technique for the production of two neutralinos in the MSSM: *anything*  $\rightarrow \tilde{\chi}_i^0 \tilde{\chi}_j^0$  ( $i, j = 2, 3, 4$ ) which subsequently decay via on- or off-shell sleptons to four leptons; here the dilepton mass edges are co-extremal with five other four-lepton invariants. Assuming the relevant SUSY spectrum is below 1 TeV and squarks/gluinos eventually decay to neutralinos, our MC study shows that one low-luminosity year at the LHC ( $10 - 30 fb^{-1}$ ) may quantitatively determine on- versus off-shell and find the relevant neutralino and slepton masses to less than 5 percent. At high luminosity ( $100 - 300 fb^{-1}$ ) these can be found to less than 1 percent.

---

<sup>1</sup>Email: nkersting@scu.edu.cn

# 1 Introduction

At a hadron collider such as the Tevatron at Fermilab or the Large Hadron Collider (LHC) at CERN, searches for New Physics (NP) states beyond the Standard Model (SM) must take into account the fact that partonic center of mass energies at these machines are not tunable (as they will be at a much anticipated  $e^+e^-$  linear collider [1]) but vary continuously in principle from zero to the combined hadronic energies of approximately 2 TeV and 14 TeV, respectively. Moreover, many NP models predict the production of a long-lived particle that is likely to escape the detectors, carrying away missing energy. The traditional method of seeing a NP mass as a sharp resonance in a cross section is therefore not applicable, and we must consider other approaches to precision measurement of NP masses crucial for testing properties of an underlying fundamental theory.

One well-studied avenue is to construct invariant mass distributions of final jet or leptonic momenta in exclusive channels and study their endpoints. Even if some NP particles carry away missing energy in each event, endpoints of said distributions can be measured and matched to analytical functions of NP masses [2]. There are several caveats to this method however. First, the exclusive channel under study must somehow be identified or assumed. Second, backgrounds must not interfere with endpoint measurement. Third, there may be some model-dependence in the method of fitting the endpoint on a 1-dimensional histogram. The first hurdle is the most difficult to clear, especially in a model such as the Minimal Supersymmetric SM (MSSM), where the gluino and squarks decay via literally hundreds of possible decay chains ("cascades"). Studies of long decay chains which have enough endpoints to solve for MSSM masses usually just focus on a few 'benchmark scenarios' [3, 4] which however may not be what Nature chooses. As for eliminating SM backgrounds, requiring a suitable number of hard jets and isolated leptons may suffice; NP backgrounds are more challenging and, if these can be reduced, typically also inflict damage in the region of the desired endpoint, where by definition rates are already low. This then brings up the third problem of how to fit the endpoint. Linear or Gaussian fits are most convenient but very detailed study of cuts and detector effects are required to understand their general accuracy [5].

The Opposite-Sign-Same-Flavor(OSSF) dilepton invariant mass is one quantity, however, which is robust in light of the caveats in the last paragraph. When a NP particle  $A$  decays as

$$A \rightarrow B l^\pm \rightarrow C l^\pm l^\mp \quad (1)$$

to  $C$  and a pair of  $l \in \{e, \mu\}$  leptons through  $B$ , the dilepton invariant mass distribution  $M_{l+l^-}$  rises linearly to its endpoint,

$$M_{l+l^-}^{max} = m_A \sqrt{1 - \frac{m_B^2}{m_A^2}} \sqrt{1 - \frac{m_C^2}{m_B^2}} \quad (2)$$

whereas if  $B$  is off-shell in this decay the distribution is not so triangular and cuts off less sharply at  $M_{l+l^-}^{max} = M_A - M_C$ . The observability of this decay chain in the MSSM, for example, where  $A$  and  $C$  are neutralinos and  $B$  is a slepton, is not too

model-dependent and simulations show that the mass edge (2) can be measured to very high ( $\sim 0.1$  GeV) precision [6], due its sharpness and low backgrounds after subtracting OSOF events that would arise with equal rates from, e.g.  $W^+W^-$  or  $t\bar{t}$ . Many of the less model-dependent NP studies are based on this mass edge: disparity between  $M_{e^+e^-}^{max}$  and  $M_{\mu^+\mu^-}^{max}$  could signal slepton nonuniversality, for example [7]. Yet the dilepton mass edge is only one function of several NP masses and cannot determine these latter.

The method of NP mass determination in the present study can be demonstrated starting from the robustness of the dilepton edge and the fact that, e.g. in the R-parity conserving MSSM, such edges come in pairs from a decay chain of the form

$$X \rightarrow A(\rightarrow B e^\pm \rightarrow C e^\pm e^\mp) \quad A'(\rightarrow B' \mu^\pm \rightarrow C' \mu^\pm \mu^\mp) \quad (3)$$

If  $X$  is a single mass eigenstate defined by  $p_X^2 \equiv m_X^2$  then the seven independent relativistically invariant contractions of four final lepton momenta can be recombined as  $M_{e^+e^-}$ ,  $M_{\mu^+\mu^-}$ , and six other invariant combinations which, when measured with high precision, can be used to solve for all the masses  $m_{X,A,B,C,A',B',C'}$ . This was done by us in [8] for the case where  $X$  was a heavy Higgs(  $H^0$  or  $A^0$ ) decaying to neutralinos ( $A = A' = \tilde{\chi}_i^0$ ,  $i = 2, 3, 4$ ) via on-shell sleptons ( $C = \tilde{e}$ ,  $C' = \tilde{\mu}$ ) to a pair of LSPs ( $C = C' = \tilde{\chi}_1^0$ ). Though we reduced model-dependence to a minimum, this cost us rate and gave rise to the aforementioned problems of fitting tails of one-dimensional histograms. We subsequently realized, however, that the dilepton invariants are highly correlated with the other invariants: at threshold( $m_X = m_A + m'_A$ ) in particular,  $(M_{e^+e^-}) \times (M_{\mu^+\mu^-})$  is co-maximal with all but one of these. If we make two or three-dimensional plots of correlations of invariants, we find these have a characteristic shape with the sought-after endpoints concentrated at one apex.

The question is now whether we can extract threshold invariants out of a superposition of (3) where  $X$  is not a single well-defined mass eigenstate but rather a continuous spectrum of such states, e.g.  $\tilde{q}\tilde{q}$ ,  $\tilde{g}\tilde{g}$ , etc. (we then ignore extra jets which may be produced in association). Though it is fairly hopeless to see distinct endpoints buried in a continuous superposition of one-dimensional histograms, we find this is not so for a superposition of multi-dimensional(we focus on  $d = 2$ ) invariant correlations: the threshold apex may not only be not buried in the superposition, but actually strengthened by it. Moreover, non-threshold endpoints can be easily extracted from the superposition, allowing us to measure a *spectrum* of invariant endpoints as functions of  $m_{X,A,B,C,A',B',C'}$ , with  $m_X$  now just an auxiliary mass which we can toss after fitting to data.

This method can be clearly generalized as follows:

1. Hypothesize a NP decay chain

$$X \rightarrow ABC\dots \rightarrow \dots \rightarrow n_j \text{ jets} + n_l \text{ leptons}$$

where  $ABC\dots$  are NP states and  $X$  is a pseudo-particle (mathematical device).

2. Form all possible invariant contractions of the  $n_j$  jet and  $n_l$  lepton momenta and derive analytical expressions for extrema of these as functions of the un-

known masses  $m_{X,A,B,C,\dots}$ . Determine which of these are co-extremal at threshold ( $m_X = m_A + m_B + m_C + \dots$ ).

3. Within each set of co-extremal invariants, construct 2- or 3-dimensional plots at threshold which make the extremal values manifest, and check this is still the case when superimposed on a non-threshold plot.

The first two steps are very straightforward (we can in fact repeat the first step with  $ABC\dots$  themselves replaced by pseudo-particles  $\zeta_1\zeta_2\zeta_3\dots$ ); only the last step seems to require some ingenuity since it depends on the kinematics of the particular decay under study. In the following analysis of neutralino pair decay to four leptons, we will, for example, discover that superimposing plots of one four-lepton invariant versus a product of two others gives rise to a 'triple-point' structure at the location of the threshold maxima. Repeating the technique with the neutralinos replaced by pseudo-particles with lower masses allows us to construct plots with a characteristic 'cat-eye' shape where the corner of the eye not only very precisely determines their threshold maxima, but actually gets sharper when non-threshold events are overlaid.

In the next section we will explain how this 'hidden threshold' technique works for a decay chain of the form (3), and in particular for the case of neutralino pair decay via sleptons. In Section 3 we then apply this technique to Monte Carlo (MC) generated data simulating a low-luminosity ( $10 - 30 \text{ fb}^{-1}$ ) run at the LHC for three different MSSM parameter points: one with on-shell decays, another with off-shell decays, and a third with an intricate combination of decays of the form (3). Finally, Section 4 summarizes these results and suggests many avenues for further application.

## 2 Invariant Mass Correlations

### 2.1 Base Case: Pure Higgs Decay

To understand the essence of our technique, one could start with the heavy Higgs decay (hereafter designated 'Higgs') to four leptons via neutralinos:

$$pp \rightarrow H/A \rightarrow \tilde{\chi}_i^0 \tilde{\chi}_j^0 \rightarrow \tilde{e}^\pm e^\mp \tilde{\mu}^\pm \mu^\mp \rightarrow e^+ e^- \mu^+ \mu^- \tilde{\chi}_1^0 \tilde{\chi}_1^0 \quad (4)$$

where the intermediate sleptons are on-shell<sup>2</sup>. We studied this decay chain in [8]; here we very briefly recapitulate. From the four observable final lepton momenta in (4) one can define seven independent invariant mass combinations. These we defined as  $M_{4l}$ ,  $\overline{M}_{2l2l}$ ,  $\overline{M}_{l3l}$ ,  $\overline{M}_{l2l}$ ,  $\overline{M}_{3l}$ ,  $\overline{M}_l$ , and  $a_4$  (please refer to that work for precise definitions of these invariants). Adding the usual dilepton invariants  $M_{e^+e^-}$  and  $M_{\mu^+\mu^-}$  to this list, we studied all distributions and derived analytic formulae for their associated endpoints. In MC simulations of LHC data ( $L = 300 \text{ fb}^{-1}$ ) at MSSM points where both neutralinos and both sleptons were degenerate, endpoint precision was unfortunately not high enough to give better than 30% determination of the

---

<sup>2</sup>It is not strictly speaking necessary to require on-shell sleptons; we will consider the less complicated case of off-shell sleptons as well in this work.

unknown masses  $m_A$ ,  $m_{\tilde{l}}$ ,  $m_{\tilde{\chi}_j^0}$ , and  $m_{\tilde{\chi}_1^0}$  in the absence of any extra information. However if one of these masses were already known to 5% accuracy, the other three could be likewise determined.

At the parameter points studied in [8] the Higgs mass was set fairly high,  $m_A \sim 400 - 600$  GeV; had these been lower, or specifically if the mass relations among the sparticles were in the order  $r_{1s} < r_{2A} < r_{2s}$  (again see [8] for definitions) we could have obtained the endpoints in a better way which forms the crux of the present technique under study. This makes use of *correlations* among the various kinematic invariants<sup>3</sup>. In particular,  $M_{4l}$ ,  $\overline{M}_{2l2l}$ ,  $\overline{M}_{l2l}$ ,  $\overline{M}_{3l}$ ,  $\overline{M}_{ll}$ , and the dilepton invariants  $M_{e^+e^-}$  and  $M_{\mu^+\mu^-}$  tend to be *simultaneously* maximal. This directly follows from the fact that when the Higgs mass is low (and in particular near threshold for neutralino pair production) these invariants are maximal for events with a particular angular configuration ([++--] in the notation of [8]; see Figure 2b of that work)<sup>4</sup>. We need only plot one invariant against another to get its maximal value, as shown in Figure 1. Note that the approach to the endpoints tends to be fairly linear along either axis, so that even with low event rates one could fit endpoints as the intersection of two lines. Another advantage is the insensitivity to backgrounds; these latter do not have the correct correlations among the various invariants and would tend to form a diffuse halo around the more concentrated signal shape. Compared to the traditional one-dimensional histogram approach, where backgrounds are harder to subtract and endpoints must be fit with a more arbitrary function, the reader can begin to appreciate that a technique using correlated invariants is much more powerful.

## 2.2 General Case

Though the technique above for the decay of a single Higgs is already applicable to many situations where one can identify a decay chain isomorphic to (4), what we would really like to do is extend our analysis to a *superposition* of decays from (hypothetical) Higgs bosons with a continuous spectrum of masses starting from a threshold mass ( $M_{ij} \equiv m_{\tilde{\chi}_i^0} + m_{\tilde{\chi}_j^0}$ ), for this is analogous to the situation at a hadron collider where the center-of-mass energy is variable.

For simplicity let us start with two different Higgs, one with threshold mass  $M_{ij}$  and the other with some higher mass  $M'$ . A plot of any invariant against another will now be a superposition of two shapes,  $\Sigma$  and  $\Sigma'$ , from events due to the threshold Higgs and higher mass Higgs, respectively, as shown in Figure 2. Suppose we are interested in finding one of the four-lepton endpoints, say  $M_{4l}$ , of events coming from the threshold Higgs decay only. If  $\Sigma$  and  $\Sigma'$  were sufficiently non-overlapping, we could just read off  $M_{4l}^{max}$  directly from a plot against another invariant, but we are to imagine the eventual limit where a continuum of shapes interpolate between  $\Sigma$

---

<sup>3</sup>The dilepton invariants  $M_{e^+e^-}$  and  $M_{\mu^+\mu^-}$  of course share a correlation in the wedgebox plot; when  $i = j$  in (4) the wedgebox plot is a box. Here we are extending this programme to more sophisticated correlations.

<sup>4</sup>Note the omission of  $\overline{M}_{l3l}$  from this list; it is odd-man-out in the sense that near threshold it is maximized by a different([+ - -+]) angular configuration.

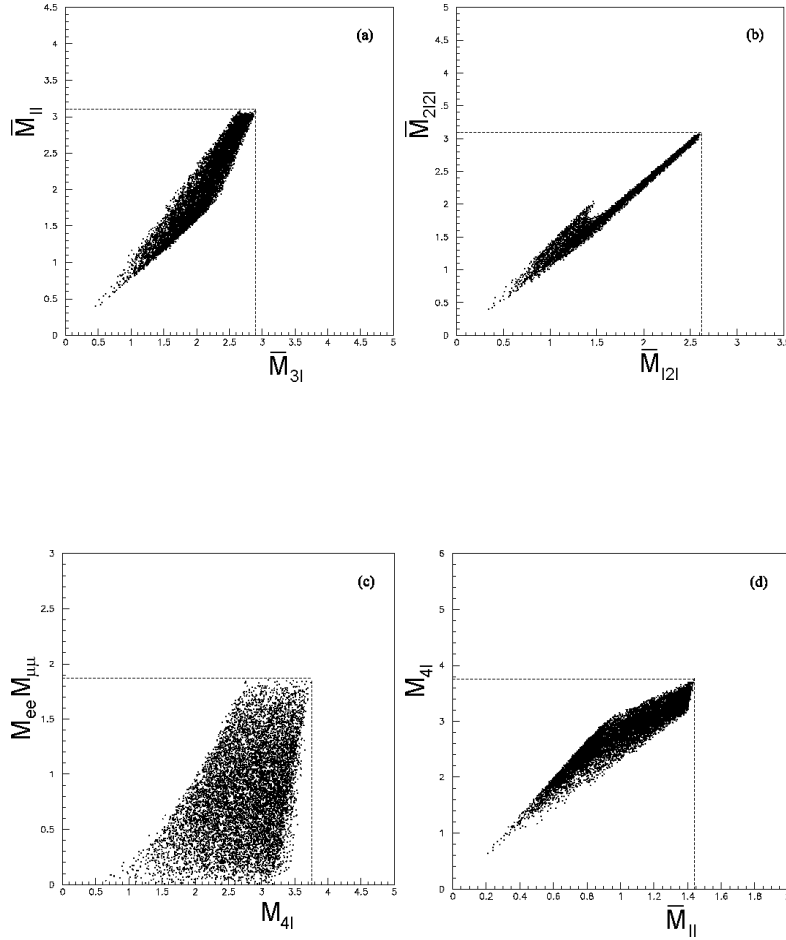


Figure 1: *Various correlations of four-lepton invariant masses at threshold ( $m_A = m_{\tilde{\chi}_i^0} + m_{\tilde{\chi}_j^0}$ ). This simulation is purely from relativistic kinematics with  $(m_{\tilde{\chi}_1^0}, m_{\tilde{\chi}_2^0}, m_{\tilde{\chi}_3^0}, m_{\tilde{l}_1^-} = m_{\tilde{l}_2^-}) = (1, 3, 4, 1.1)$  (units arbitrary). Dashed lines mark the maximum value of each invariant.*

and  $\Sigma'$  and the tip of  $\Sigma$  will be hidden in the superposition. We might as well start with a plot against  $(M_{e^+e^-}) \times (M_{\mu^+\mu^-})$  (which can in turn be read off with high precision from a wedgebox plot) where the tip  $P$  of  $\Sigma$  is in fact always hidden in the superposition with  $\Sigma'$  (Figure 2a). The reason for this is that  $(M_{e^+e^-}) \times (M_{\mu^+\mu^-})$  is maximal for four different angular configurations:  $[+ + - -]$ ,  $[+ - - -]$ ,  $[- + - -]$ , and  $[- - - -]$  (same-flavor leptons are emitted back-to-back in each of these cases). Meanwhile  $M_{4l}$  is maximal for  $[+ + - -]$  only (see Appendix for exact expression) and attains the lower value of  $2M_{e^+e^-}^{max}$  or  $2M_{\mu^+\mu^-}^{max}$  for the other configurations; this left-most corner of the shape in Figure 2a therefore contains no new information. A

similar situation applies to the other invariants as well, e.g.  $\overline{M}_{3l}$ (Figure 2b) where the desired point  $Q$  can only be said to lie somewhere along the top edge of  $\Sigma + \Sigma'$ . However if we plot a triple product such as  $(\overline{M}_{3l}) \times (M_{e^+e^-}) \times (M_{\mu^+\mu^-})$  against  $M_{4l}$  and vice versa the flatness of this edge is raised(see Figure 2(c,d)) and  $P$  and  $Q$  may even jut out from  $\Sigma + \Sigma'$  if  $M'$  is sufficiently high. In any case  $P$  and  $Q$  are now uniquely defined by consistency: the values of  $\overline{M}_{3l}^{max}$  and  $M_{4l}^{max}$  at  $P$  must agree with those at  $Q$  for the *same* value of  $(M_{e^+e^-}) \times (M_{\mu^+\mu^-}) = (M_{e^+e^-}^{max}) \times (M_{\mu^+\mu^-}^{max})$ . This consistency check proves crucial in the following.

When a continuum of Higgs with masses ranging from  $M_{ij}$  upwards to  $M'$  decay, the threshold shape  $\Sigma$  is completely obscured in the superposition (which still looks very much like Figures 2(c,d)), but its upper edge remains intact; indeed it is reinforced by all the other decays' shapes. Though we can't directly see  $P$  and  $Q$ , we know they must lie somewhere on this edge of the combined shape and satisfy the consistency check among  $M_{4l}^{max}$ ,  $\overline{M}_{3l}^{max}$ , and  $(M_{e^+e^-}^{max}) \times (M_{\mu^+\mu^-}^{max})$ : this still uniquely defines them. The other simultaneously maximal invariants  $\overline{M}_{2l2l}$ ,  $\overline{M}_{l2l}$ , and  $\overline{M}_{ll}$  can be found in an identical fashion by plotting in pairs against  $(M_{e^+e^-}) \times (M_{\mu^+\mu^-})$  and performing consistency checks. We could also plot them in triplets against each other, iterating consistency checks among the plots of  $\overline{M}_{l2l}$  vs.  $(\overline{M}_{ll}) \times (\overline{M}_{2l2l})$ ,  $\overline{M}_{ll}$  vs.  $(\overline{M}_{2l2l}) \times (\overline{M}_{ll})$ , and  $\overline{M}_{2l2l}$  vs.  $(\overline{M}_{ll}) \times (\overline{M}_{l2l})$  in cyclic order, obtaining three more threshold points  $R$ ,  $S$ , and  $T$ (see Figures 2(e,f,g)).

What is perhaps not so obvious at first is that any point  $X$  on the edge of the combined shape *below*  $P$  in Figure 2c also satisfies a consistency check with point  $Y$  in Figure 2d, but for a lower value of  $(M_{e^+e^-}^{max})' \times (M_{\mu^+\mu^-}^{max})' < (M_{e^+e^-}^{max}) \times (M_{\mu^+\mu^-}^{max})$ . Yet this must be true by inductive reasoning, since the relationship between  $\Sigma$  and the encompassing  $\Sigma'$  must also hold between some  $\Sigma''$  which is in turn encompassed by  $\Sigma$ . A graphically convenient way to obtain  $X$  and  $Y$  for a given  $(M_{e^+e^-}^{max})' \times (M_{\mu^+\mu^-}^{max})'$  is to superimpose a plot of  $M_{4l}$  vs.  $\overline{M}_{3l} \frac{(M_{e^+e^-}) \times (M_{\mu^+\mu^-})}{(M_{e^+e^-}') \times (M_{\mu^+\mu^-}' )}$  with one of  $M_{4l} \frac{(M_{e^+e^-}) \times (M_{\mu^+\mu^-})}{(M_{e^+e^-}') \times (M_{\mu^+\mu^-}' )}$  vs.  $\overline{M}_{3l}$  (superimpose Figure 2c and Figure 2d with swapped and rescaled axes). This gives rise to a characteristic 'cat-eye' shape(Figure 2h), where the upper corner of the eye pinpoints the correct extrema of  $M_{4l}$  and  $\overline{M}_{3l}$  (one would first perform linear fits in the vicinity of  $X$  and  $Y$  and note their intersection on the cat-eye plot). Evidently  $X$  and  $Y$  correspond to a pseudo-resonance with mass less than  $M_{ij}$  decaying at threshold to a pair of auxiliary particles  $\zeta_1\zeta_2$ , which then decay as usual through on-shell sleptons. Regardless of whether this resonance or auxiliary particles actually exist, it remains mathematically correct to say that every point on the edge of the combined shape corresponds to a different set of invariant endpoints  $(M_{e^+e^-}') \times (M_{\mu^+\mu^-}')$ ,  $M_{4l}^{max'}$ ,  $\overline{M}_{2l2l}^{max'}$ ,  $\overline{M}_{l2l}^{max'}$ ,  $\overline{M}_{3l}^{max'}$ , and  $\overline{M}_{ll}^{max'}$  which depend on the masses  $m_1, m_s, m_{\zeta_1}$  and  $m_{\zeta_2}$  (see Appendix). We may choose any such point, figure out what  $(M_{e^+e^-}') \times (M_{\mu^+\mu^-}')$  has to be for consistency (or vice versa with a cat-eye plot), measure the other endpoints at this pseudo-threshold, and invert them to find  $m_1, m_s, m_{\zeta_1}$  and  $m_{\zeta_2}$ . At any point away from an actual physical threshold,  $m_{\zeta_1}$  and  $m_{\zeta_2}$  are just auxiliary parameters which we can set equal for convenience; however at  $P$  we must have  $m_{\zeta_{1,2}} = m_{\tilde{\chi}_{i,j}^0}$ . Since there is no limit in

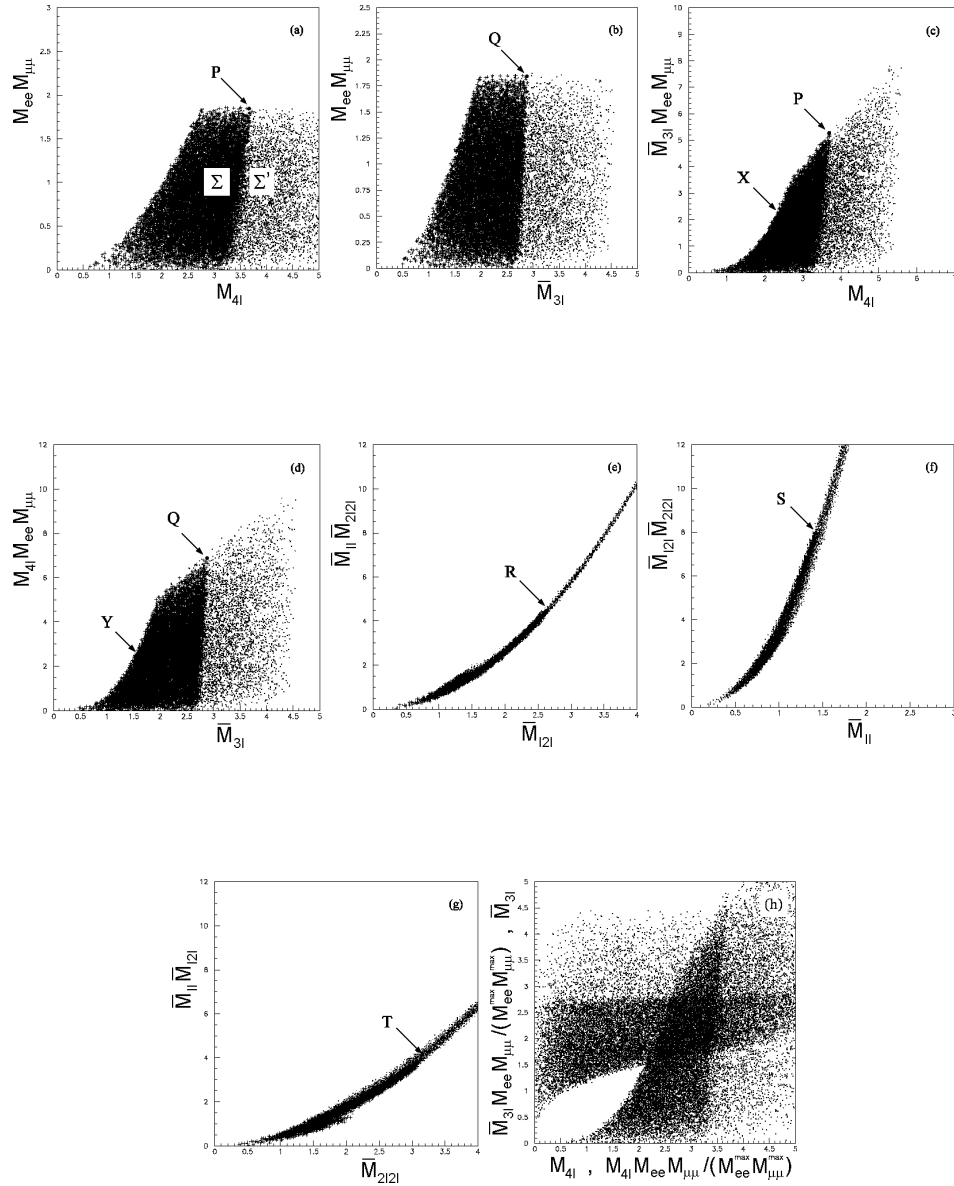


Figure 2: *Superposition of two different Higgs decays  $4$ , one with threshold mass ( $= 7$  in arbitrary units) and one with a higher mass ( $= 8$ ), giving rise to two shapes  $\Sigma$  and  $\Sigma'$ . Other masses are as in Figure 1. The threshold shape  $\Sigma$  is plotted in a darker symbol for clarity, though in reality  $\Sigma$  and  $\Sigma'$  would consist of one indistinguishable whole. Points  $P, Q, R, S, T$  denote positions at which threshold invariants are maximal.  $P$  and  $Q$  may be found by a consistency check between (c) and (d), while  $R, S,$  and  $T$  may likewise be found among the highly constrained shapes in (e), (f) and (g). In (h) we show a typical 'cat-eye' plot constructed for a pseudo-resonance  $X$  and  $Y$  in (c) and (d).*



principle to the number of pseudo-thresholds and therefore of cat-eye plots, we can combine fits from several of these to reconstruct slepton and LSP masses, as well as  $m_{\tilde{\chi}_{i,j}^0}$  from the dilepton edge formula (2), to high precision.

Thus, in the present example, a tight correlation among the threshold and pseudo-threshold maxima of  $M_{4l}$ ,  $\overline{M}_{2l2l}$ ,  $\overline{M}_{12l}$ ,  $\overline{M}_{3l}$ , and  $\overline{M}_{ll}$  ensures that they, and the SUSY masses they depend on, can be found with high precision for a sufficiently large collection of events. Though high rates to neutralinos may be hard to achieve for exclusive Higgs decay channels, it should be no problem via inclusive channels at the LHC if the relevant SUSY spectrum lies below 1 TeV: colored cascades from even a moderately-massive ( $\lesssim 800$  GeV) gluino and squarks should lead to copious production of neutralino pairs which may decay to leptons, i.e.

$$X \rightarrow X' + \tilde{\chi}_i^0 (\rightarrow \tilde{e}^\pm e^\mp \rightarrow e^+ e^- \tilde{\chi}_1^0) \tilde{\chi}_j^0 (\rightarrow \tilde{\mu}^\pm \mu^\mp \rightarrow \mu^+ \mu^- \tilde{\chi}_1^0) \quad (5)$$

Here  $X$  could be  $pp$ ,  $\tilde{q}\tilde{q}'$ ,  $\tilde{q}\tilde{g}$ ,  $\tilde{g}\tilde{g}$ ,  $\tilde{\chi}_2^\pm \tilde{\chi}_2^\mp$  etc., or any two<sup>5</sup> SUSY particles with a continuous center of mass energy greater than or equal to  $M_{ij}$ , while  $X'$  are any collection of particles that do not confuse the 4-lepton signal. As long as one or more neutralino-pair subchains are intact, the mother chain is irrelevant. Note also we do not require the lightest neutralino to be stable, as long as its decay products do not include leptons. As we shall see in the next section this technique works very well in MC simulations with a minimal requirement of four isolated leptons plus missing energy.

### 3 Application to Neutralino Decays

In this section we demonstrate the robustness of our technique for neutralino decays at three different MSSM parameter points with varying decay topologies. Our MC setup uses HERWIG 6.5 and private codes as in our previous publications [8, 9, 10] and the reader is referred to these for details.

We generate events

$$pp \rightarrow \{\tilde{q}, \tilde{g}, \tilde{\chi}^\pm, \tilde{\chi}^0\} \{\tilde{q}, \tilde{g}, \tilde{\chi}^\pm, \tilde{\chi}^0\} \quad (6)$$

for  $10\text{--}30$   $fb^{-1}$  (a low-luminosity year at the LHC) and only pass those which decay to a hard and isolated  $e^+e^-$  and  $\mu^+\mu^-$  pair with sufficient missing energy ( $E_T^{\text{miss}} > 20$  GeV). This eliminates SM backgrounds aside from  $pp \rightarrow Z^*Z$ , though this can be modeled and subtracted (by a Z-veto if necessary). SUSY backgrounds fall into two categories: those which produce exactly four leptons and those which produce more than this (presumably losing some to isolation cuts, detector effects, etc.). The first category includes slepton or chargino '3+1' decays such as  $\tilde{\chi}_i^\pm (\rightarrow l^\pm l'^\pm l'^\mp \nu \nu' \bar{\nu}') \tilde{\chi}_1^0) \tilde{\chi}_j^\mp (\rightarrow l''^\mp \nu'' \tilde{\chi}_1^0)$  where one decay goes to three leptons and the other to one. These could always be substantially reduced via flavor subtraction, but this is not necessary since they do not obscure the structure in the vicinity of a '2+2' threshold point. In the

---

<sup>5</sup>The present work assumes R-parity is exact, though the general technique does not require this.

case where '3+1' decays significantly outnumber '2+2' decays, we would just derive endpoints for this decay topology instead and match against a trilepton invariant mass edge. Such backgrounds should therefore be considered an 'enriched signal.' The second category of SUSY backgrounds includes events such as  $\tilde{\tau}\tilde{\tau}$  where each stau decays  $\tilde{\tau} \rightarrow \tau\tilde{\chi}_2^0 \rightarrow l^\pm l'^\pm l'^\mp \nu\nu'\tilde{\chi}_1^0$  and two of the total of six leptons are somehow lost. Yet such events, if not made utterly small by leptonic branching fractions, would introduce a more-or-less diffuse halo in our correlation plots, and in particular should not confuse the identification of threshold points.

### 3.1 On-Shell Box

The most basic example of the full application of our technique is for the decay (5) where  $i = j$ . A  $\tilde{\chi}_2^0\tilde{\chi}_2^0$  pair, for example, is often the chief product of colored cascades at mSUGRA points, e.g. SPS1a. Though we have checked our technique works at SPS1a, we choose another point which has higher rates and therefore better demonstrates the agreement with theory presented in the last section.

#### On-Shell Point

$$\begin{aligned} \mu &= 250 \text{ GeV} & M_2 &= 250 \text{ GeV} & M_1 &= 125 \text{ GeV} \\ \tan\beta &= 10 & M_{\tilde{e},\tilde{\mu},L\tilde{\tau}} &= 250 \text{ GeV} & M_{\tilde{e},\tilde{\mu}R} &= 130 \text{ GeV} \\ M_A &= 700 \text{ GeV} & M_{\tilde{g}} &\approx 400 \text{ GeV} & M_{\tilde{b}} &\approx 500 \text{ GeV} \end{aligned}$$

Here we have raised the left-handed slepton and stau soft mass inputs above those of the right-handed selectron and smuon (note the physical masses differ slightly from these, see Table 1) to suppress sneutrino exchange and stau modes which may reduce the magnitude of (but not character of) the signal. The heavy Higgs mass is set rather high to remove it from the analysis, but setting it lower would in fact be beneficial since it contributes to the signal process *anything*  $\rightarrow \tilde{\chi}_i^0\tilde{\chi}_j^0$ .

With a luminosity of  $30 \text{ fb}^{-1}$  the wedgebox plot in Figure 3a is a very dense and symmetric box structure, which confirms degenerate neutralinos decaying via degenerate sleptons<sup>6</sup>. The dilepton mass distribution (Figure 3b) is quite triangular, suggesting the sleptons are on-shell — in the next subsection we will show a quantitative proof of this fact. Notice there is some extraneous wedge-like structure from chargino and heavier neutralino decays outside the main box bounded at  $\sim 75 \text{ GeV}$ , but as we shall see now this helps rather than hinders us. Figure 3(c,d) show the correlation between  $M_{4l}$ ,  $\overline{M}_{3l}$ , and  $(M_{e^+e^-}) \times (M_{\mu^+\mu^-})$ : the threshold points  $P$  and  $Q$  are immediately obvious as a sort of 'triple point' structure with the aforementioned 'extraneous' points assisting in this identification. We can visually mark  $P$  and  $Q$  to a couple  $\text{GeV}$  or so, and using the consistency check determine them to sub-GeV precision. Threshold values of  $\overline{M}_{2l2l}$ ,  $\overline{M}_{l2l}$ , and  $\overline{M}_{ll}$  may be similarly determined, refining them if desired via tri-correlations as in Figure 2(e,f,g). These endpoints

<sup>6</sup>Strictly speaking this could also be a chargino decaying via a sneutrino, i.e.  $\tilde{\chi}_2^\pm \rightarrow l^\pm\tilde{\nu} \rightarrow l^\pm l'^\mp \tilde{\chi}_1^\pm$ . Other signs such as the number of 6-lepton events (after  $\tilde{\chi}_1^\pm \rightarrow l^\pm \nu \tilde{\chi}_1^0$ ) might resolve this ambiguity.

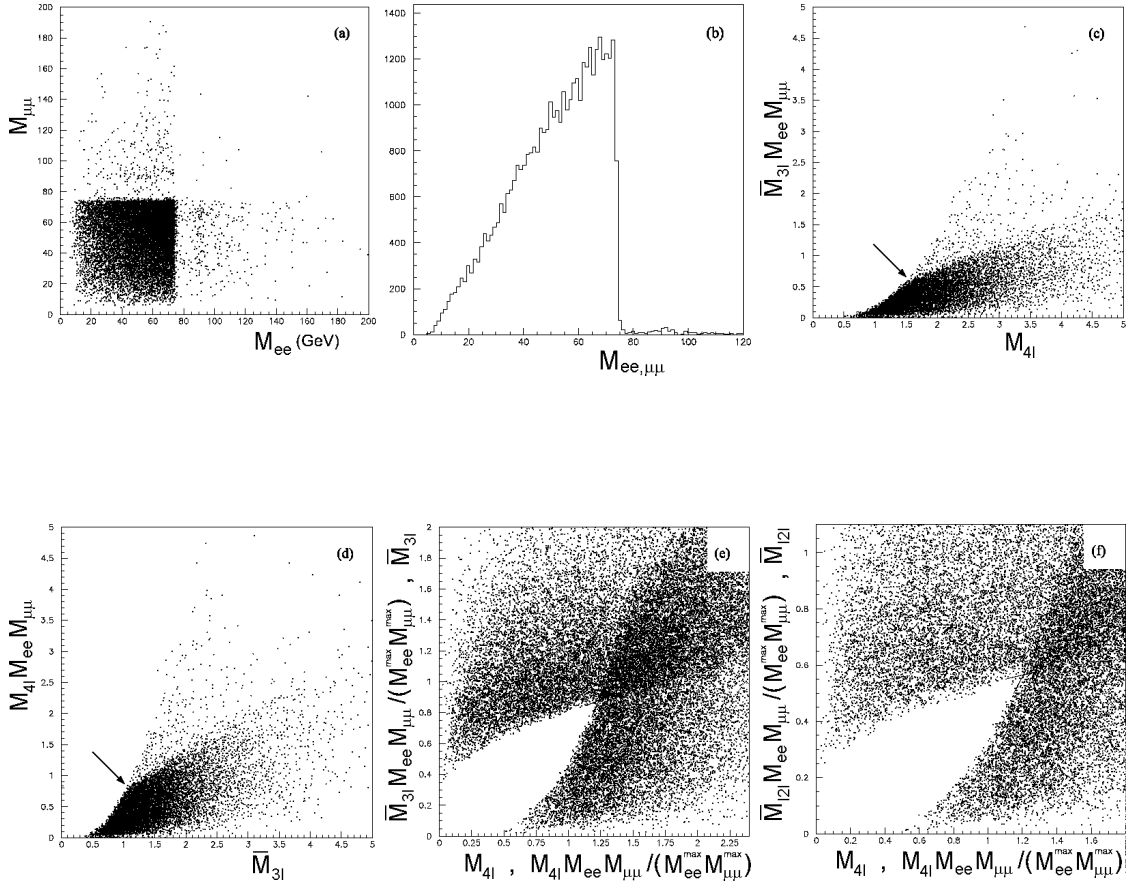


Figure 3: Various plots for the On-Shell Point with  $30 \text{ fb}^{-1}$  luminosity. The wedgebox plot (a) is very box-like (with some wedge-like structure on the outskirts) with a triangular dilepton mass distribution (b) typifying an on-shell decay. The threshold values of  $M_{4l}$  and  $\overline{M}_{3l}$  for the  $\tilde{\chi}_2^0 \tilde{\chi}_2^0$  resonance in (c,d) are easy to locate (in this and all following plots, axis units are in units of  $100 \text{ GeV}$  or  $100 \text{ GeV}^2$ ). A lower, pseudo-threshold can be analyzed with a 'cat-eye' plot (e): this is constructed by making linear fits at the desired point in (c,d) and then overlapping the (rescaled) plots. Plots for other invariants, e.g.  $\overline{M}_{12l}$  in (e), are very similar.

can therefore all be determined with sub-GeV precision, and we estimate that ultimately, with over  $100 \text{ fb}^{-1}$  luminosity, to  $0.1 \text{ GeV}$  precision. Yet even with this level of precision the inversion of endpoint formulae (see Appendix) does not yield a unique solution ( $m_{\tilde{\chi}_1^0}$ ,  $m_{\tilde{t}}$ ,  $m_{\tilde{\chi}_2^0}$ ) (hereafter we abbreviate these as  $m_1$ ,  $m_s$ ,  $m_2$ ). This is because the endpoint formulae are highly nonlinear and generically give a discrete set of eight or more solutions.

Table 1: *Relevant masses at the On-Shell Point, Off-Shell Point, and Mixed Point (all masses in GeV).*

	$\tilde{\chi}_1^0$	$\tilde{\chi}_2^0$	$\tilde{\chi}_3^0$	$\tilde{\chi}_4^0$	$\widetilde{e}_R, \widetilde{\mu}_R$	$\tilde{\chi}_1^\pm$	$\tilde{\chi}_2^\pm$
On-Shell	117.1	197.5	257.2	317.7	134.7	193.3	317.0
Off-Shell	79.6	131.5	160.6	249.5	148.0	115.6	249.0
Mixed	94.2	144.8	166.0	277.1	109.7	144.0	277.7

However, note that the edge below threshold in Figure 3(c,d) is very dense and hence amenable to a cat-eye analysis. Figures 3(e,f) show cat-eye plots constructed for a dilepton edge of  $(M_{e^+e^-}^{max})' = (M_{\mu^+\mu^-}^{max})' = 60$  GeV. The other endpoints for this pseudo-threshold can be determined by the intersection of linear fits (in red) to very high ( $< 0.1$  GeV) precision owing to our freedom in choosing the precise values of auxiliary masses here. Combining the cat-eye solution with the real threshold solution above, and assuming 0.5 GeV precision on these latter, now gives  $m_1$ ,  $m_s$ , and  $m_2$  to within  $\pm 6$  GeV of their nominal values in Table 1. In the high luminosity ( $100 - 300 fb^{-1}$ ) limit, all masses can be found to  $\pm 2$  GeV.

### 3.2 Off-Shell Box

Decays through off-shell sleptons are simpler for two reasons. First, mathematically speaking, invariant mass edges do not depend on slepton masses; in the case of a box topology these can therefore only depend on  $m_1$  and  $m_j$ . Since the dilepton mass edge is equal to the difference of these, we only need one other function of these masses to determine them.

Secondly, the physical degrees of freedom are easier to analyze: for threshold decays in particular, each neutralino  $\tilde{\chi}_j^0$  is at rest in the center of mass frame and leptonic invariants are maximized/minimized when the same flavor leptons are emitted antiparallel/parallel. The product  $(M_{e^+e^-}) \times (M_{\mu^+\mu^-})$  is therefore maximal when the electron(muon) is antiparallel to the positron(anti-muon), and is equal to  $(m_j - m_1)^2$ . For this kinematical configuration, however, all the other invariants  $M_{4l}$ ,  $\overline{M}_{2l2l}$ ,  $\overline{M}_{l2l}$ ,  $\overline{M}_{3l}$ , and  $\overline{M}_{ll}$  are equal (up to a constant factor) to  $(m_j - m_1)$  and therefore do not provide independent information.

The trick is to consider configurations where the electron and positron are antiparallel while the muon and anti-muon are parallel (or vice versa). In this case  $M_{e^+e^-}$  or  $M_{\mu^+\mu^-}$  is maximal and the other invariants (excepting  $\overline{M}_{l2l}$ ) unconditionally attain *minima*:

$$M_{4l}^{min} = (m_j - m_1) \sqrt{2 + \frac{m_1}{m_j}} \quad (7)$$

$$\overline{M}_{2l2l,3l,ll}^{min} = (m_j - m_1) \left( \frac{\alpha + \beta \frac{m_1}{m_j} + \gamma \frac{m_1^2}{m_j^2}}{\xi} \right)^{\frac{1}{4}} \quad (8)$$

Table 2: *Offshell Decay Parameters in (8) and Fits to MC data at the Off-Shell Point for the LSP mass ( $m_1$ ), assuming the dilepton edges are exact and 0.2 GeV precision on other endpoints. Also shown are attempted fits to data at the On-Shell Point which, even with larger( $\pm 1$  GeV) errors, give self-inconsistent results.*

Invariant	$\alpha$	$\beta$	$\gamma$	$\xi$	LSP(Off)	LSP(On)
$M_{4l}^{min}$	4	4	1	1	$85 \pm 5$	$22 \pm 5$
$\overline{M}_{2l2l}^{min}$	2	1	0	1	$85 \pm 11$	$172 \pm 78$
$\overline{M}_{3l}^{min}$	11	10	3	8	$84 \pm 6$	$1 \pm 5$
$\overline{M}_l^{min}$	3	2	1	48	$86 \pm 15$	$-8 \pm 10$

for specific values of the parameters  $\alpha$ ,  $\beta$ ,  $\gamma$ , and  $\xi$  listed in Table 2. Thus any one of these in conjunction with the dilepton mass edge uniquely determines  $m_j$  and  $m_1$ . Geometrically these endpoints are the intersections of the line  $M_{l+l^-} = (m_j - m_1)$  with the near edges of the shapes on a plot versus  $M_{4l}$ ,  $\overline{M}_{2l2l}$ ,  $\overline{M}_{3l}$ , or  $\overline{M}_l$ . These intersections can be found with high precision and then checked against each other for consistency.

To see the efficacy of this method, consider the following

### Off-Shell Point

$$\begin{aligned}
 \mu &= 150 \text{ GeV} & M_2 &= 200 \text{ GeV} & M_1 &= 100 \text{ GeV} \\
 \tan \beta &= 10 & M_{\widetilde{e,\mu,L}\widetilde{\tau}} &= 300 \text{ GeV} & M_{\widetilde{e,\mu_R}} &= 135 \text{ GeV} \\
 M_A &= 700 \text{ GeV} & M_{\widetilde{q}} &\approx 300 \text{ GeV} & M_{\widetilde{g}} &\approx 350 \text{ GeV}
 \end{aligned}$$

Though the  $10 \text{ fb}^{-1}$  wedgebox plot in Figure 4a looks very similar to that of the On-Shell Point, the dilepton edge at  $M_{l+l^-}^{max} = 51.9 \text{ GeV}$  is in fact due to three-body decays via off-shell sleptons. We might guess this from the vaguely less-than-triangular distribution in Figure 4b, but now we have a better way. Simply intersecting the  $M_{l+l^-} = M_{l+l^-}^{max}$  line with each shape in Figures 4(c,d,e,f), we find endpoints that can be matched against the formulae in (7) and (8). Table 2 shows that these give mutually consistent values of  $m_1$  and  $m_j$ , which at high luminosity may be determined to a percent or so. Had we constructed the same plots at our On-Shell Point (which look very similar), we would have also obtained a set of endpoints as well, but these all give inconsistent, even nonsensical values for  $m_{1,j}$  (e.g., a negative LSP mass!). Though the dilepton distributions of Figures 3a,4a give qualitative hints of whether sleptons are on- or off-shell, here we seem to have the first definitively *quantitative* method of determining this which succeeds even with modest (several GeV) endpoint precision.

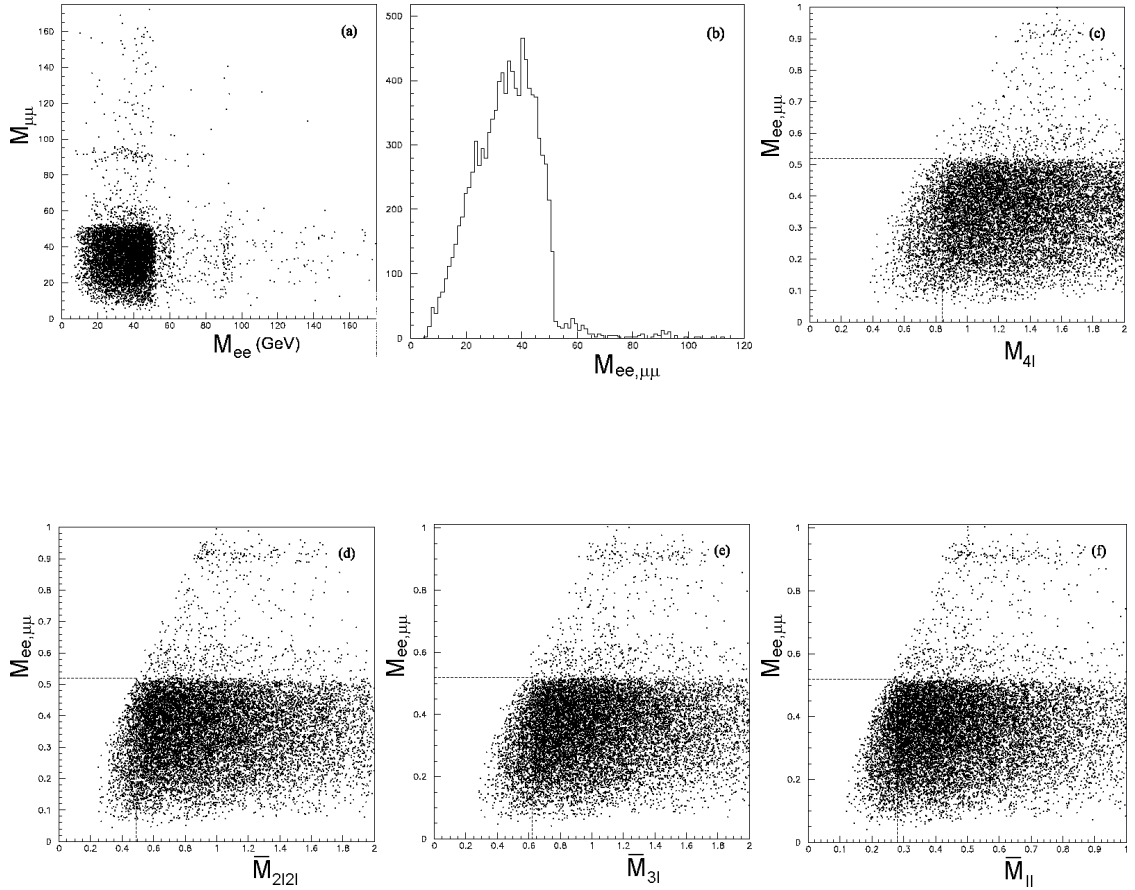


Figure 4: *MC Simulation at the Off-Shell Point for  $10 \text{ fb}^{-1}$  luminosity. The wedgebox plot in (a) is a very crisp box (though not without hints of extra wedgelike structure and decays through on-shell  $Z$  bosons) whose (b) dilepton invariant mass shape is not quite triangular. (c – f) show where the dilepton maximum is coincident with various minima of the other invariants; these are then matched against formulae (7) and (8); see Table 2 for results.*

### 3.3 Mixed Topology

Now consider a much more complicated example at the following MSSM parameter point:

#### Mixed Point

$$\begin{aligned}
 \mu &= -150 \text{ GeV} & M_2 &= 250 \text{ GeV} & M_1 &= 100 \text{ GeV} \\
 \tan \beta &= 5 & M_{\widetilde{e}, \widetilde{\mu}, L, \widetilde{\tau}} &= 200 \text{ GeV} & M_{\widetilde{e}, \widetilde{\mu}, R} &= 120 \text{ GeV} \\
 M_A &= 700 \text{ GeV} & M_{\widetilde{q}} &\approx 500 \text{ GeV} & M_{\widetilde{g}} &\approx 400 \text{ GeV}
 \end{aligned}$$

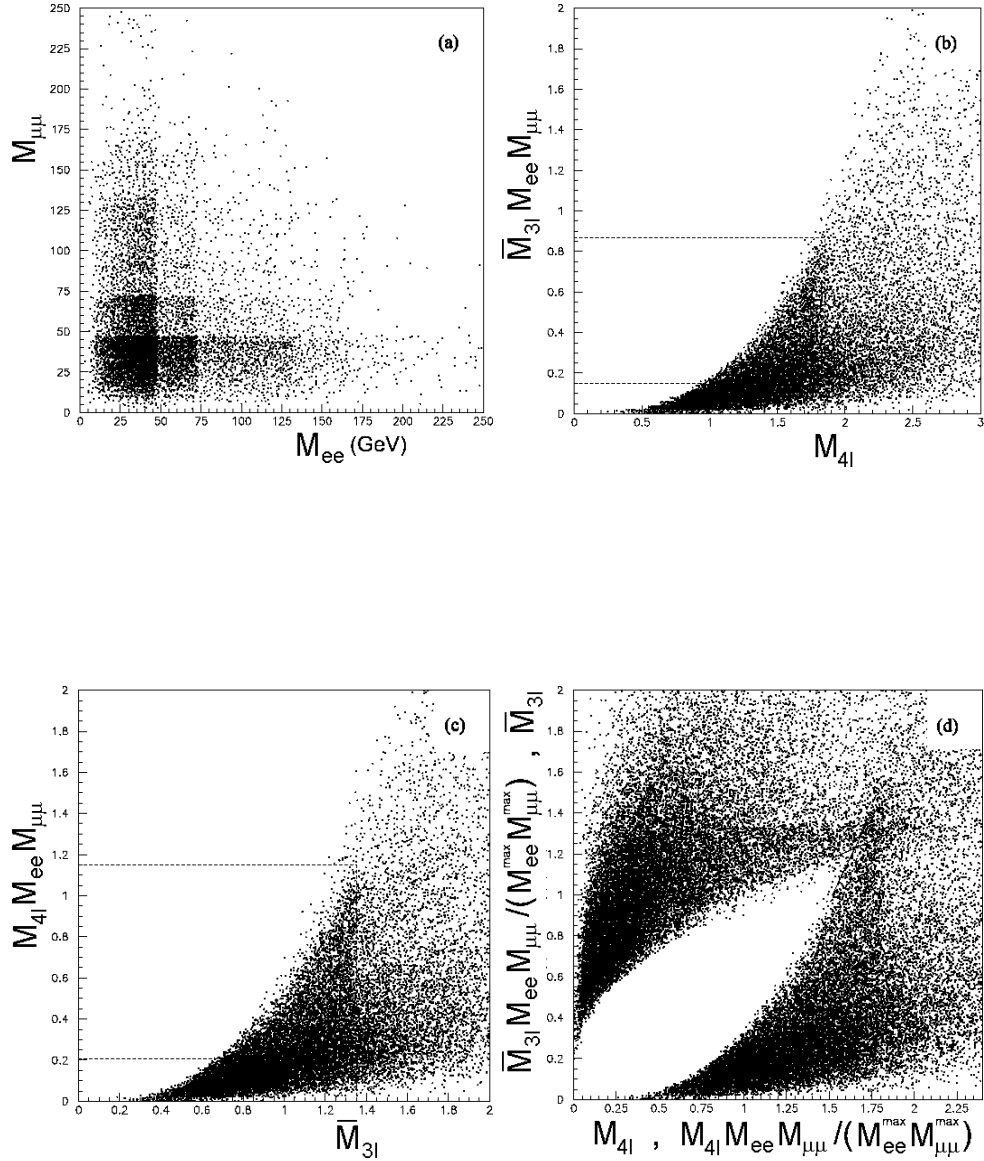


Figure 5: For the Mixed Point at  $30 \text{ fb}^{-1}$ , a very complicated wedgebox plot (a) results, but the inner box within  $\sim 45 \text{ GeV}$  is probably from  $\tilde{\chi}_2^0$  decays. At least two threshold points can be visually marked in (b) and (c), the former corresponding to a  $\tilde{\chi}_2^0 \tilde{\chi}_2^0$  resonance, the latter to  $\tilde{\chi}_2^0 \tilde{\chi}_2^\pm$ . Assuming the dilepton edge at  $\sim 70 \text{ GeV}$  is from  $\tilde{\chi}_3^0$  decays to the LSP, the  $\tilde{\chi}_3^0 \tilde{\chi}_3^0$  threshold point can be found via a cat-eye plot (d) constructed from this value.

From the  $30 \text{ fb}^{-1}$  wedgebox plot of Figure 5a we can mark at least four dilepton edges at  $M_{l+l-} \approx 45, 70, 130,$  and  $160 \text{ GeV}$ , all of which must be left open to interpre-

tation at this point<sup>7</sup>. However we can safely conjecture that the lowest and sharpest edge at 45.6 GeV is from  $\tilde{\chi}_2^0 \rightarrow l^\pm \tilde{l}^\mp \rightarrow l^+ l^- \tilde{\chi}_1^0$ , where we could use the method of the last section to determine this is indeed an on-shell decay. The threshold point for this  $\tilde{\chi}_2^0 \tilde{\chi}_2^0$  channel is easily located in Figure 5(b,c) near  $M_{4l} \approx 100$  GeV for example, and with a precision of 0.5 GeV combined with a cat-eye plot for a point below threshold we can determine  $m_1$ ,  $m_s$ , and  $m_2$  to within about  $\pm 14$  GeV of their nominal values in Table 1. With a higher luminosity measurement of this threshold to 0.2 GeV these masses can be found with an accuracy of  $\pm 6$  GeV.

There is also a strong edge at  $M_{l+l^-} = 71.9$  GeV; we might posit this is due to  $\tilde{\chi}_3^0 \rightarrow l^\pm \tilde{l}^\mp \rightarrow l^+ l^- \tilde{\chi}_1^0$ , and if so we can just solve for  $m_3$  from the dilepton edge formula (2) since we have already determined the LSP and relevant slepton mass. Yet we should check this value of  $m_3$  by constructing a cat-eye plot for  $(M_{e^+e^-}) \times (M_{\mu^+\mu^-}) = 71.9 \times 71.9$  GeV<sup>2</sup> (corresponding to a  $\tilde{\chi}_3^0 \tilde{\chi}_3^0$  resonance) or  $45.6 \times 71.9$  GeV<sup>2</sup> (for a  $\tilde{\chi}_2^0 \tilde{\chi}_3^0$  resonance) and seeing if the measured values of  $M_{4l}$ ,  $\overline{M}_{2l2l}$ , etc. agree with what is expected; agreement for both of these is indeed intact, so our guess was correct.

Let us go further and assume the fainter edge near  $\sim 130$  GeV is due to  $\tilde{\chi}_4^0 \rightarrow l^\pm \tilde{l}^\mp \rightarrow l^+ l^- \tilde{\chi}_1^0$ . Going through the same procedure we find, however, results inconsistent with the above values of  $m_1$ ,  $m_s$ , and  $m_2$ . How about  $\tilde{\chi}_4^0 \rightarrow l^\pm \tilde{l}^\mp \rightarrow l^+ l^- \tilde{\chi}_2^0$  then? The cat-eye plot for this choice of  $(M_{e^+e^-}) \times (M_{\mu^+\mu^-}) \approx 45.6 \times 130$  GeV<sup>2</sup> then comes together very close to the conspicuous second threshold point in Figure 5b near  $(M_{4l}, \overline{M}_{3l}) \approx (180, 90)$  GeV, so this seems to be promising. However, scanning over  $(m_1, m_s, m_2, m_4)$  for a match to these endpoints subject to constraints from the first threshold measurements proves negative, even if we assign large ( $\pm 5$  GeV) errors to the invariants. Accessing the MC output file shows that this edge arises from  $\tilde{\chi}_2^\pm \rightarrow l^\pm \tilde{\nu} \rightarrow l^+ l^- \tilde{\chi}_1^\pm$ ; since the masses of  $\tilde{\chi}_{1,2}^\pm$  are nearly the same as those for  $\tilde{\chi}_{2,4}^0$  our guess of the latter gave us nearly the same threshold point, but the intermediate particle is not a charged slepton ( $m_s \approx 110$  GeV) in this case but rather a sneutrino ( $m_{sn} \approx 200$  GeV). To deduce this from an actual data set one might apply a hidden threshold technique to other SUSY processes such as  $\tilde{\chi}_{1,2}^\pm \tilde{\chi}_{1,2}^\pm$  or  $\tilde{\nu} \tilde{\nu}$  for particular decay chains and see whether the extracted values of masses give consistent results.

A complicated superposition of decay topologies at this Mixed Point therefore generically requires several complementary analyses. However it can also be said that there is a tremendous amount of information to be mined here.

## 4 Conclusions

Let us now summarize the hidden resonance technique and how we applied it in this work:

1. DEFINE the decay chain  $X \rightarrow ABC\dots \rightarrow n_j$  jets +  $n_l$  leptons +  $Y$ , where  $X$  is anything and  $Y$  is exclusive of jets and leptons. *In our case this was  $X \rightarrow \tilde{\chi}_i^0 \tilde{\chi}_j^0$*

---

<sup>7</sup>For example, aside from the simplest possibilities  $\tilde{\chi}_i^0 \tilde{\chi}_j^0$  where each neutralino decays to two leptons, we should also consider  $\tilde{\chi}_1^0 \tilde{\chi}_4^0 (\rightarrow e^+ e^- \tilde{\chi}_2^0 (\rightarrow \mu^+ \mu^- \tilde{\chi}_1^0))$ , and  $\tilde{\chi}_2^0 \tilde{\chi}_2^\pm (\rightarrow l^\pm \tilde{\nu} (\rightarrow l^\mp \tilde{\chi}_1^\pm))$ .



where each neutralino then decayed via a slepton to a pair of OSSF leptons and the LSP.

2. DERIVE analytic expressions for all jet and lepton invariant mass endpoints as functions of NP masses, and find kinematic configurations for which two or more of these are co-extremal. *In our case of four leptons ( $n_l = 4$ ), there are in principle 7 independent invariants; of these, we found  $(M_{e^+e^-}) \times (M_{\mu^+\mu^-})$ ,  $M_{4l}$ ,  $\overline{M}_{2l2l}$ ,  $\overline{M}_{l2l}$ ,  $\overline{M}_{3l}$ , and  $\overline{M}_{ll}$  were simultaneously maximal for on-shell decays, whereas for off-shell decays  $M_{l+l-}$  was maximal where  $M_{4l}$ ,  $\overline{M}_{2l2l}$ ,  $\overline{M}_{3l}$ , and  $\overline{M}_{ll}$  were minimal. Deriving analytical formulae for these extrema was not difficult since most of the work had already been done in [8]. The formalism of that work can be used to compute extrema for any chain of two- and three-body decays.*
3. DISPLAY correlations of the above invariants in a plot which makes their extremal values visually obvious, hence easily computable. *For off-shell slepton decays it sufficed to plot each invariant versus  $M_{l+l-}$  and note the intersection with the line  $M_{l+l-} = M_{l+l-}^{max}$ . For on-shell decays we found it useful to plot one invariant against another times  $(M_{e^+e^-}) \times (M_{\mu^+\mu^-})$  and look for a threshold point, visually obvious by its 'triple point' structure, refining with a consistency check. We also could look at points below threshold using the 'cat-eye' plot technique; this amounts to repeating our technique for the decay chain  $X \rightarrow \zeta_1\zeta_2 \rightarrow e^\pm\tilde{e}^\mp\mu^\pm\tilde{\mu}^\mp$  where now we have three pseudo-particles  $X$ ,  $\zeta_{1,2}$ .*

Note that in the above, "extremal" can be interchanged for "geometrically identifiable", since it is certainly conceivable that some other feature of a threshold decay such as a peak or a kink is visually enhanced by non-threshold decays.

To demonstrate the general applicability of this technique to NP, we present below a (incomplete)spectrum of examples. Each example in itself entails numerous variations(e.g. on-shell intermediate states could likewise be taken off-shell):

- Heavy Higgs Decay:  $H/A \rightarrow \tilde{\chi}_i^0(\rightarrow e^+e^-\tilde{\chi}_1^0)\tilde{\chi}_j^0(\rightarrow \mu^+\mu^-\tilde{\chi}_1^0)$ . As considered in [8], but augmented by the case where  $H/A$  is replaced by a pseudo-resonance with mass  $m_i + m_j$ .
- Sneutrino Pair Production:  $\tilde{\nu}\tilde{\nu}(\rightarrow l^\pm\tilde{\chi}_1^\mp(\rightarrow \tilde{\chi}_0W^-(\rightarrow l'^\mp\nu')))$  Here  $n_l = 4$  as for neutralino pair production, but with totally different kinematics: one can analogously define  $M_{4l}$ ,  $\overline{M}_{2l2l}$ ,  $\overline{M}_{l3l}$ , etc., though threshold extrema of these will have a different correlation.
- Neutralino Decay via higgs:  $\tilde{\chi}_2^0\tilde{\chi}_2^0(\rightarrow \tilde{\chi}_1^0h(\rightarrow bb))$ . This  $n_j = 4$  decay is a potential competitor to the sleptonic modes considered in this paper.
- Chargino Pair Production:  $\tilde{\chi}_2^\pm\tilde{\chi}_2^\mp(\rightarrow l^\mp\tilde{\nu}(\rightarrow l^\pm\tilde{\chi}_1^\mp(\rightarrow l^\mp\nu\tilde{\chi}_1^0)))$  This is a  $n_l = 6$  case which means there are as many as 45 relativistic invariants<sup>8</sup>.

---

<sup>8</sup>The number of invariants is computed as the number of pairwise contractions among the available momenta, as well as with powers of  $\epsilon^{\mu\nu\rho\sigma}$

- Slepton Pair Production  $\tilde{l}^\pm \tilde{l}^\mp (\rightarrow l^\mp \tilde{\chi}_2^0 (\rightarrow l^\pm l^\mp \tilde{\chi}_1^0))$ . This could either be  $n_l = 6$  or  $n_l = 4$  depending on whether the other slepton decays similarly or directly to the LSP, respectively.
- Squark Pair Production  $\tilde{q}\tilde{q} (\rightarrow q\tilde{\chi}_2^0 (\rightarrow l^\pm \tilde{l}^\mp (\rightarrow l^\mp \tilde{\chi}_1^0)))$ . A  $n_j = 2, n_l = 4$  decay.
- Gluino Pair Production  $\tilde{g}\tilde{g} (\rightarrow q\tilde{q} (\rightarrow q\tilde{\chi}_2^0 (\rightarrow q'q'\tilde{\chi}_1^0)))$  This  $n_j = 8$  decay has an astounding 588 invariants.
- Nonstandard Higgs decays  $h \rightarrow XY$  (e.g. [11])
- Exotic Vectors (from, e.g. Little Higgs [12])
- Kaluza-Klein Pair Production (e.g. [13]).
- Exotica decays to top-pairs  $pp \rightarrow X \rightarrow t\bar{t}$  (e.g. [14])
- Low-Scale Technicolor (e.g.  $W^\pm \pi_T \rightarrow l^\pm \nu b\bar{b}$  [15]).

The hidden threshold method provides another way to see signatures of these NP models and determine any unknown masses involved. Results can be made even stronger in combination with inclusive techniques and complementary methods of mass determination (in SUSY for example, see [6, 16, 17]). We hope that research along these lines will allow an earlier discovery of NP at hadron colliders.

## References

- [1] Linear Collider Collaboration, "Precision measurement of a particle mass at the linear collider." arXiv:0712.4389 [hep-ph]
- [2] H. Bachaco, I. Hinchliffe, and F. E. Paige, "Measurements of masses in SUGRA models at LHC." Phys.Rev.**D62**:015009 (2000).
- [3] B.C. Allenbach et al., "The Snowmass points and slopes: Benchmarks for SUSY searches," In: N. Graf (ed.), Snowmass 2001: Proc. of APS/DPF/DPB Summer Study on the Future of Particle Physics, Snowmass, Colorado, July, 2001, page 125, arXiv: 0202233 [hep-ph]. Eur. Phys. J. C **25**: 113 (2002)
- [4] B.K. Gjelsten, D.J. Miller, and P. Osland. "Measurement of the gluino mass via cascade decays for SPS 1a." JHEP **0506**:015 (2005).
- [5] D.J. Miller, P. Osland, and A.R. Raklev, "Invariant mass distributions in cascade decays." JHEP **0603**:034,2006.
- [6] "ATLAS Detector and Physics Performance Technical Design Report 2", Chapter 20, CERN-LHCC-99-015, ATLAS-TDR-15, May, 1999, <http://atlas.web.cern.ch/Atlas/GROUPS/PHYSICS/TDR/access.html>

- [7] B.C. Allanach, J.P. Conlon, and C.G. Lester, "Measuring Smuon-Selectron Mass Splitting at the LHC and Patterns of Supersymmetry Breaking." arXiv:0801.3666 [hep-ph]
- [8] P. Huang, N. Kersting, and H.H. Yang, "Model-Independent SUSY Masses from 4-Lepton Kinematic Invariants at the LHC." arXiv:0801.0041 [hep-ph].
- [9] G. Bian, M. Bisset, N. Kersting, Y. Liu, and X. Wang, "Wedgebox analysis of four-lepton events from neutralino pair production at the LHC." Eur.Phys.J.**C53**:429-446 (2008).
- [10] M. Bisset, N. Kersting, J. Li, F. Moortgat, S. Moretti, and Q.L. Xie, "Pair-produced heavy particle topologies: MSSM neutralino properties at the LHC from gluino/squark cascade decays." Eur.Phys.J.**C45**:477-492 (2006).
- [11] S. Chang, R. Dermisek, J.F. Gunion, and N. Weiner, "Nonstandard Higgs Boson Decays." arXiv:0801.4554 [hep-ph]
- [12] M. Schmaltz, and D. Tucker-Smith, "Little Higgs review." Ann. Rev. Nucl. Part. Sci.**55**: 229-270 (2005)
- [13] P. Nath, Y. Yamada, and M. Yamaguchi, "Probing the Nature of Compactification with Kaluza-Klein Excitations at the Large Hadron Collider." Phys.Lett. **B466** : 100-106 (1999)
- [14] R. Frederix and F. Maltoni, "Top pair invariant mass distribution: A Window on new physics." arXiv:0712.2355 [hep-ph]
- [15] E. Eichten and K. Lane, "Low-scale technicolor at the Tevatron and LHC." arXiv:0706.2339 [hep-ph]
- [16] H.-C. Cheng, J. F. Gunion, Z. Han, G. Marandella, and B. McElrath, "Mass determination in SUSY-like events with missing energy." JHEP **0712**:076 (2007).
- [17] K. Kawagoe, M.M. Nojiri, and G. Polesello, "A New SUSY mass reconstruction method at the CERN LHC." Phys.Rev.**D71**:035008 (2005).

## Appendix

Threshold maxima for on-shell decays are readily computed via the methodology of [8]. For the case  $i = j$  we just substitute  $m_A = 2m_j$  in the formulae of that work for the  $[+ + - -]$  configurations, obtaining the following:

$$\mathbf{M}_{41}^{\max} = \frac{m_1^2 m_j^2 - 2m_j^2 m_s^2 + m_s^4}{-m_j m_s^2};$$

$$\mathbf{M}_{2121}^{\max} = \frac{1}{3^{1/4} m_j m_s^2} (3m_1^8 m_j^8 - 4m_1^6 m_j^6 m_s^2 (2m_j^2 + m_s^2) - 4m_1^2 m_j^2 m_s^6 (8m_j^6 - 12m_j^4 m_s^2 + 6m_j^2 m_s^4 + m_s^6) + m_s^8 (16m_j^8 - 32m_j^6 m_s^2 + 24m_j^4 m_s^4 - 8m_j^2 m_s^6 + 3m_s^8) + 6m_1^4 (4m_j^8 m_s^4 - 4m_j^6 m_s^6 + 3m_j^4 m_s^8))^{1/4};$$

$$\overline{M}_{121}^{\max} = \frac{1}{6^{1/4}m_j m_s^2} (3m_1^8 m_j^8 - 2m_1^6 m_j^6 m_s^2 (5m_j^2 + m_s^2) + 6m_1^4 m_j^4 m_s^4 (3m_j^4 - m_j^2 m_s^2 + m_s^4) - 2m_1^2 m_j^2 m_s^6 (8m_j^6 - 6m_j^4 m_s^2 + 3m_j^2 m_s^4 + m_s^6) + m_s^8 (8m_j^8 - 16m_j^6 m_s^2 + 18m_j^4 m_s^4 - 10m_j^2 m_s^6 + 3m_s^8))^{1/4};$$

$$\overline{M}_{31}^{\max} = \frac{(m_1^4 m_j^4 - 2m_1^2 m_j^4 m_s^2 + 2m_j^4 m_s^4 - 2m_j^2 m_s^6 + m_s^8)^{1/4} \sqrt{m_1^2 m_j^2 - 2m_j^2 m_s^2 + m_s^4}}{2^{1/4} m_j m_s^2};$$

$$\overline{M}_{11}^{\max} = \frac{\sqrt{m_1^4 m_j^4 - 2m_1^2 m_j^4 m_s^2 + 2m_j^4 m_s^4 - 2m_j^2 m_s^6 + m_s^8}}{24^{1/4} m_j m_s^2};$$